Systematic Changes in Cloud Radiative Forcing with Aerosol Loading for Deep Clouds in the Tropics

JIE PENG

State Key Laboratory of Earth Surface Processes and Resource Ecology, College of Global Change and Earth System Science, Beijing Normal University, Beijing, and Shanghai Institute of Meteorological Science, Shanghai Meteorological Bureau, Shanghai, China

ZHANQING LI

Earth System Science Interdisciplinary Center, and Department of Atmospheric and Oceanic Science, University of Maryland, College Park, College Park, Maryland, and State Key Laboratory of Earth Surface Processes and Resource Ecology, College of Global Change and Earth System Science, Beijing Normal University, Beijing, China

HUA ZHANG

Laboratory for Climate Studies, National Climate Center, China Meteorological Administration, Beijing, China

JIANJUN LIU

Earth System Science Interdisciplinary Center, and Department of Atmospheric and Oceanic Science, University of Maryland, College Park, College Park, Maryland, and State Key Laboratory of Earth Surface Processes and Resource Ecology, College of Global Change and Earth System Science, Beijing Normal University, Beijing, China

MAUREEN CRIBB

Earth System Science Interdisciplinary Center, and Department of Atmospheric and Oceanic Science, University of Maryland, College Park, College Park, Maryland

(Manuscript received 6 March 2015, in final form 1 September 2015)

ABSTRACT

It has been widely recognized that aerosols can modify cloud properties, but it remains uncertain how much the changes and associated variations in cloud radiative forcing are related to aerosol loading. Using 4 yr of A-Train satellite products generated from *CloudSat*, the *Cloud–Aerosol Lidar and Infrared Pathfinder Satellite Observations* satellite, and the *Aqua* satellite, the authors investigated the systematic changes of deep cloud properties and cloud radiative forcing (CRF) with respect to changes in aerosol loading over the entire tropics. Distinct correlations between CRF and aerosol loading were found. Systematic variations in both shortwave and longwave CRF with increasing aerosol index over oceans and aerosol optical depth over land for mixed-phase clouds were identified, but little change was seen in liquid clouds. The systematic changes are consistent with the microphysical effect and the aerosol invigoration effect. Although this study cannot fully exclude the influence of other factors, attempts were made to explore various possibilities to the extent that observation data available can offer. Assuming that the systematic dependence originates from aerosol effects, changes in CRF with respect to aerosol loading were examined using satellite retrievals. Mean changes in shortwave and longwave CRF from very clean to polluted conditions ranged from -192.84 to $-296.63\,\mathrm{W\,m^{-2}}$ and from 18.95 to $46.12\,\mathrm{W\,m^{-2}}$ over land, respectively, and from -156.12 to $-170.30\,\mathrm{W\,m^{-2}}$ and from 6.76 to $11.67\,\mathrm{W\,m^{-2}}$ over oceans, respectively.

1. Introduction

By acting as cloud condensation nuclei (CCN) and/or ice nuclei, aerosols affect Earth's energy budget through the modification of cloud properties, which is often

Corresponding author address: Prof. Zhanqing Li, Earth System Science Interdisciplinary Center, 5825 University Research Court, Suite 4001, College Park, MD 20740-3823.
E-mail: zli@atmos.umd.edu

DOI: 10.1175/JAS-D-15-0080.1

referred to as the aerosol indirect effect (AIE) (Twomey 1977; Albrecht 1989; Ramaswamy et al. 2001; Lohmann and Feichter 2005; Tao et al. 2012). A greater number of smaller cloud droplets formed in a dirty environment suppresses collision and coalescence processes and thus delays or inhibits rainfall. This suppression has been investigated using measurements made during several aircraft campaigns in different regions around the world, including tropical clouds in the Amazon (Andreae et al. 2004), hail storms in Argentina (Rosenfeld et al. 2006), a winter storm in California (Rosenfeld et al. 2008b), winter clouds in Israel, and summer monsoon clouds in India (Freud and Rosenfeld 2012). Comparing the relationship between visibility and precipitation at Hua Mountain and stations on the neighboring plain in central China, Yang et al. (2013a,b) found that both orographic precipitation and summer thunderstorms were suppressed by aerosols. Camponogara et al. (2014) also found that rainfall over the La Plata basin was suppressed by aerosols.

As a result of rain suppression, clouds made up of smaller droplets may reach higher levels in the atmosphere. Once the freezing level is reached, ice processes begin, and more latent heat is released to invigorate the vertical development of the cloud. This phenomenon is referred to as the aerosol invigoration effect (AIV), which has been observed from aircraft measurements (Andreae et al. 2004), satellite data (Koren et al. 2005; Lin et al. 2006; Niu and Li 2012; Storer et al. 2014), and long-term ground observations (Li et al. 2011). The effect has been modeled with cloud-resolving models (Khain and Pokrovsky 2004; Khain et al. 2005, 2008; Wang 2005; Seifert and Beheng 2006; Tao et al. 2007; Fan et al. 2007, 2009, 2012; Van den Heever et al. 2011) and explained by a conceptual theory proposed by Rosenfeld et al. (2008a) and a revised theory (Fan et al. 2013). Whether aerosols invigorate or suppress cloud and thunderstorms seems to depend on the joint effects of aerosol radiative and microphysical effects: suppression for absorbing aerosols and enhancement for hygroscopic aerosols (Yang et al. 2013a,b; Yang and Li 2014).

Both observational and modeling studies have shown that the AIV can lead to changes in cloud geometry, precipitation, lighting activities, and even the strength of tropical cyclones. Midweek peaks in lighting frequency and the probability of severe convective storms seen during the summer in the eastern United States have been observed to coincide with peaks in the amount of anthropogenic aerosols (Bell et al. 2009; Rosenfeld and Bell 2011). Rosenfeld et al. (2007) hypothesized that the AIV could lead to the convergence of air into the eyewalls of tropical cyclones, which would decrease maximum wind speeds. This was supported by observations of how variations in aerosols accounted for an 8% variation in the intensity of Atlantic hurricanes (Rosenfeld et al. 2011). Wang et al. (2014) have also shown that both precipitation and net cloud radiative forcing (CRF) over the northwestern Pacific are enhanced by Asian pollution via the invigoration of winter cyclones. A review of aerosol effects on the intensity and microphysics of tropical cyclones has been given by Rosenfeld et al. (2012), while a review of general aerosol effects on convective clouds and precipitation has been summarized by Tao et al. (2012).

While the AIV and ensuing effects have been studied extensively, few studies have been done on the radiative forcing (RF) associated with the AIV. Koren et al. (2010) have simulated the RF of tropical deep convective clouds. The influence of aerosols showed up in several ways. For a thick convective cloud where the albedo effect of the cloud is nearly saturated, the negative effect induced by aerosols was small. The invigoration effect can cause cloud tops to reach greater heights while keeping their albedo fixed at the nearly saturated value for thick clouds. The colder cloud tops emit less thermal radiation to space, so they induce a positive RF. However, for optically thinner clouds, both shortwave (SW) and longwave (LW) forcing can be strong. The AIV can produce warming or cooling based on the particular combination of macro- and microphysical properties (Koren et al. 2010). At night, however, warming due to the AIV can be very strong, leading to a daily mean net warming effect (Fan et al. 2012). Aerosols are involved in the expansion of anvils through the aerosol microphysical effect rather than the AIV, which produces more semitransparent ice clouds (Fan et al. 2013). This causes a strong positive RF (Yan et al. 2014). The overall net radiative effect associated with the AIV is a function of three cloud parameters (height, extent, and microphysics) and their diurnal variations. A call for further studies to investigate this net effect was made at a recent World Climate Research Programme Climate Science meeting (Rosenfeld et al. 2013).

Niu and Li (2012) analyzed 1 yr of A-Train (L'Ecuyer and Jiang 2010) satellite data and found systematic variations in cloud-top height and thickness associated with aerosol loading over the global tropical oceans and land. These dependencies are consistent with the findings of Li et al. (2011), who used long-term (10 yr) ground-based measurements. They also used a wide variety of other observation data and model simulations to investigate if the dependencies were driven by anything other than aerosols. These studies demonstrate that use of a large ensemble of data

TABLE 1. Summary of satellite products and model datasets used in the study.

Geophysical parameter	Product	Satellite and sensor	Spatial resolution
Cloud geometry	2B-GEOPROF-lidar	*CloudSat* cloud profiling radar (CPR) and *CALIPSO* CALIOP	Horizontal: 1.4 km × 2.5 km Vertical: 240 m
Cloud ice water, cloud liquid water	2B-CWC-RVOD	*CloudSat* CPR	Horizontal: 1.4 km × 2.5 km Vertical: 240 m
Atmospheric temperature profiles	ECMWF-AUX	—	Horizontal: 1.4 km × 2.5 km Vertical: 240 m
Column water vapor	ECMWF-AUX	—	Horizontal: 1.4 km × 2.5 km Vertical: 240 m
Lower-troposphere static stability	ECMWF-AUX	—	Horizontal: 1.4 km × 2.5 km Vertical: 240 m
Relative humidity	ECMWF-AUX	—	Horizontal: 1.4 km × 2.5 km Vertical: 240 m
Cloud radiative forcing	2B-FLXHR	*CloudSat* CPR	Horizontal: 1.4 km × 2.5 km Vertical: 240 m
Aerosol optical depth, Ångström exponent	MYD08	*Aqua* MODIS	Horizontal: 1° × 1° Vertical: —

collected over a long period of time or over a large domain can suppress the influence of atmospheric dynamics on observed relationships between aerosols and clouds.

The present study follows an approach similar to that used by Yan et al. (2014) but uses multiyear global satellite data instead of long-term ground-based measurements made at one location. We examine the systematic changes in CRF with increasing aerosol loading over the entire tropics, where deep convective clouds are more plentiful than at higher latitudes and where different types of aerosols under varying meteorological conditions are present. These systematic changes are referred to as aerosol-mediated changes in CRF (AMCRF; Rosenfeld et al. 2013). Four years of satellite data from both active and passive sensors onboard different satellites composing the A-Train are used. This study is also a natural extension of the study by Niu and Li (2012), which revealed systematic variations in cloud geometry with aerosol loading using 1 yr of A-Train merged data. Besides using a much larger dataset, this study focuses on the impact of aerosols on the CRF, whereas the study by Niu and Li (2012) was only concerned with the impact of aerosols on clouds and precipitation.

The findings of Niu and Li (2012) are first verified with the extended set of satellite data, which helps reduce statistical uncertainties. The main goal of the study is to investigate the variation in CRF with aerosol loading so that insight into the AMCRF can be gained. The possible dependence of the CRF on the aerosol index (AI) and aerosol optical depth (AOD) are investigated over oceans and land, respectively. Section 2 describes the datasets and methodology used in the study. Results are presented in section 3, and conclusions are given in section 4.

2. Data and methodology

Four years (2007–10) of cloud data (NASA CloudSat Project 2007) from the *CloudSat* and the *Cloud–Aerosol Lidar and Infrared Pathfinder Satellite Observations* (*CALIPSO*) satellites and aerosol data (NASA Goddard Space Flight Center 2008) from the Moderate Resolution Imaging Spectroradiometer (MODIS) onboard the *Aqua* platform over the global tropics (20°N–20°S) are used. This region was chosen because of the ubiquitous presence of convective clouds, for which the AIV is more significant. The horizontal resolution of the cloud products is 1.4 km × 1.1 km, and the vertical resolution is 240 m. MODIS aerosol products include the level 3 AOD at 550 nm and the Ångstrom exponent (AE) gridded over 1° × 1° boxes. The gridded data were generated by averaging level 2 data, which shows good agreement with ground-based observations (e.g., Chu et al. 2005; Li et al. 2007; Mi et al. 2007; Levy et al. 2007, 2010). Table 1 summarizes all products used.

A limitation of studying collocated aerosols and clouds from space is the problem of cloud contamination (Marshak et al. 2008; Yang et al. 2012). Through use of a combination of MODIS and Advanced Spaceborne Thermal Emission and Reflection Radiometer data, Wen et al. (2007) found that AOD derived using a one-dimensional retrieval assumption can be strongly enhanced by three-dimensional reflectance from neighboring clouds This enhancement arises from multiple factors, such as the distance between clear and cloudy pixels, the optical properties of surrounding

TABLE 2. Fractional distribution of AOD values over the domain considered in this study from 2007 to 2010.

	AOD						
Year	0.0–0.1	0.1–0.2	0.2–0.3	0.3–0.4	0.4–0.5	0.5–0.6	>0.6
2007	0.292	0.396	0.157	0.065	0.034	0.019	0.036
2008	0.312	0.390	0.149	0.063	0.034	0.019	0.033
2009	0.323	0.386	0.150	0.063	0.033	0.018	0.028
2010	0.316	0.392	0.147	0.061	0.032	0.018	0.035

TABLE 3. Definitions of cloud type.

	Warm-base mixed-phase clouds	Cold-base mixed-phase clouds	Liquid clouds
Cloud-base temperature (°C)	>15°	0°–15°	>0°
Cloud-top temperature (°C)	<−4°	<−4°	>0°

clouds, the wavelength, and the surface albedo. Aerosol properties can be affected by clouds located up to 15 km away, with the strongest effect at low latitudes (Varnai and Alexander 2011). *CloudSat* data were averaged over 1° × 1° grids to match MODIS data. Values of AOD > 0.6 are excluded to reduce the possibility of cloud contamination in AOD retrievals. Cloud contamination tends to increase the magnitude of AOD. Chances are that, in a cloudy scene, higher AOD values likely include a contribution from cloud contamination. So use of small AOD would be a way of reducing the chance of cloud contamination. We calculated the PDF of AOD over the entire tropical region from 2007 to 2010 (see Table 2) and found that more than 96% of AOD values are less than 0.6, and more than 90% of AOD values are less than 0.4. A somewhat ad hoc choice of AOD = 0.6 is thus selected in this study to ensure that a sufficient number of samples are retained for statistical analyses and that the problem of cloud contamination is minimized. Although AOD is often used as a proxy for CCN, AI, defined as the product of AOD and AE, is a better proxy because aerosol particle size information is included (Nakajima et al. 2001; Feingold et al. 2006). Because of the unreliability of the AE retrieval from MODIS over land (Levy et al. 2010), AI and AOD were used as proxies for aerosol loading over oceans and land, respectively.

Following Peng et al. (2014), *CloudSat* products were used to identify all single-layer deep clouds and to obtain their mean properties, as well as to obtain meteorological parameters. Mean cloud-top heights (CTH) and cloud-base heights (CBH) of all single-layer cloudy profiles were extracted from the *CloudSat* geometric profile lidar product (2B-GEOPROF-lidar). Temperatures at cloud base (CBT) and cloud top (CTT) were extracted from the European Centre for Medium-Range Weather Forecasts (ECMWF) auxiliary (ECMWF-AUX) product. Other variables extracted from the ECMWF-AUX product include relative humidity (RH) profiles, column water vapor (CWV), and lower-tropospheric static stability (LTSS), which is defined as the potential temperature (PT, calculated from temperature and pressure data derived from the ECMWF-AUX) difference between the surface and the 700-hPa pressure level ($PT_{surface} - PT_{700\text{-}hPa}$) (Klein and Hartmann 1993). The mean of the difference between saturated specific humidity and ambient specific humidity (VaporD) at the 500- and 700-hPa levels was computed using CWC information (Redelsperger et al. 2002). Instantaneous values for CRF were obtained from the *CloudSat* radiative fluxes and heating rate (2B-FLXHR) product; and ice water path (IWP), liquid water path (LWP), liquid effective radius (LER), and ice effective radius (IER) were obtained from the *CloudSat* radar-visible optical depth cloud water content (2B-CWC-RVOD) product. For grid boxes containing multiple values of AOD/AI, mean values were calculated.

CBT and CTT were used to define three cloud types that have significantly different responses to the AIV (Li et al. 2011; Niu and Li 2012): warm-base mixed-phased (WBM) clouds, cold-base mixed-phase (CBM) clouds, and liquid clouds. Table 3 lists the criteria used to identify these clouds. Note that, for any one grid box, the CBT and CTT used are the mean values of CBT and CTT for all single-layer clouds within the grid box. All cloud samples were divided into different AOD and AI bins (see Table 4). They were then analyzed to determine how CRF at the top of the atmosphere (TOA) and related cloud properties change with increases in AI or AOD.

3. Results

a. *The impact of AIV on CRF and related cloud properties*

Figure 1 shows correlations between CTT, CTH, and cloud thickness (CTK) with AOD over land and AI over oceans for different cloud types. As reported by Li et al. (2011) and Niu and Li (2012), there are systematic variations in CTT, CTH, and CTK as aerosol loading increases. Compared with those obtained from 1 yr of A-Train data over the same region (Niu and Li 2012), the relationships are more statistically significant, with much smaller standard errors, as shown by

TABLE 4. Number of samples in different AI and AOD bins.

Ocean/AI bin	Liquid clouds	Warm-base mixed-phase clouds	Cold-base mixed-phase clouds	Land/AOD bin	Liquid clouds	Warm-base mixed-phase clouds	Cold-base mixed-phase clouds
0.0000–0.0152	3595	28	77	0–0.1	8159	459	1119
0.0152–0.0231	6500	44	99	0.1–0.2	1646	1118	2292
0.0231–0.0351	12 429	80	212	0.2–0.3	5976	855	1763
0.0351–0.0534	22 304	181	395	0.3–0.4	2204	442	927
0.0534–0.0811	31 956	420	882	0.4–0.5	1117	239	449
0.0811–0.1233	31 748	662	1180	0.5–0.6	655	125	282
0.1233–0.1874	15 444	500	881	—	—	—	—
0.1874–0.2848	4396	197	345	—	—	—	—
0.2848–0.4329	1900	69	139	—	—	—	—
0.4329–0.6579	699	26	40	—	—	—	—

the error bars computed as the standard error (SE), given by

$$\mathrm{SE} = \frac{\mathrm{SD}}{\sqrt{N}},$$

where SD is the standard deviation of the data falling in an AOD or AI bin, and N is the sample number in each bin. Note that some of the error bars are very small because N is large. This will help reduce uncertainties in estimates of AMCRF. For mixed-phase clouds, CTH and CTK are positively correlated with AI or AOD, while CTT is negatively correlated. Note that the increases (decreases) in CTH and CTK (CTT) are more significant when AOD ≤ 0.3 and become much weaker for larger AOD. This is consistent with results from previous studies by Rosenfeld et al. (2008a) and Ten Hoeve et al. (2012). This can be explained by the two primary effects of aerosol: namely, the radiative effect and invigoration effect. The former is due to aerosol scattering and absorption of solar radiation, which reduce solar radiation reaching the surface and, consequently, sensible heat flux to suppress convection, while the invigoration is just the opposite. As aerosol loading becomes larger, its radiative effect becomes stronger and exceeds the invigoration (microphysical) effect, resulting in an overall inhibition effect. Yan et al. (2014) showed that, when the wind shear (vertical velocity) is large (small), the dependence of CTT on AOD for deep convective clouds is weak. No obvious correlation is found in the case of liquid clouds. A stronger dependence is seen for WBM clouds than for CBM clouds. This is presumably because more latent heat is released in WBM clouds as more water cloud droplets are converted into ice crystals. This release of extra energy helps clouds develop higher into the atmosphere. If CTT and CTK are considered as proxies for the strength of convection, it is not surprising to see that convection is stronger over land than over ocean. Not only are the CTH and CTK over land larger than those over oceans, the relative changes from clean to polluted conditions are also systematically larger over land than over oceans. In general, the AIV is more pronounced over regions with strong convection (Khain et al. 2005; Fan et al. 2009; Tao et al. 2012). The striking contrast in the apparent dependence of cloud geometry on aerosol loading is revealing because the formation and development of clouds share much in common in terms of the atmospheric setting but differ considerably in terms of cloud microphysics. Significant differences in their responses to aerosol loading due to latent heat release, as illustrated by Rosenfeld et al. (2008a), would arise. If the dependence was the act of a third factor, for which aerosols serve as a proxy, this factor may respond differently to the three types of clouds shown in Fig. 1. Despite numerous tests using both observation and modeling data (Li et al. 2011; Niu and Li 2012; Fan et al. 2013; Yan et al. 2014), this elusive third factor has not been found, which is further demonstrated below.

Figure 2 shows IWP, LWP, IER, and LER as a function of AOD over land and AI over ocean. As expected, there are strong positive correlations between IWP/IER and AI/AOD. The increases in IWP and IER are weaker again when AOD exceeds 0.3. Similar to the effect on cloud geometry and consistent with Niu and Li (2012), the strongest correlation is seen for WBM clouds over land where bin-mean IWP values range from 1151 to 2131 $\mathrm{g\,m^{-2}}$ as AOD increases from (0–0.1) to (0.5–0.6) (Fig. 2a). Likewise, mean IER increases from 80.4 to 85.1 μm when conditions go from clean to polluted (Fig. 2c).

Jiang et al. (2011) found that both convective strength and aerosol loading can affect the IER for deep convective clouds. To examine this, we used IWP as a proxy of convective strength and plotted IER in WBM and CBM clouds as a function of AOD and AI for different

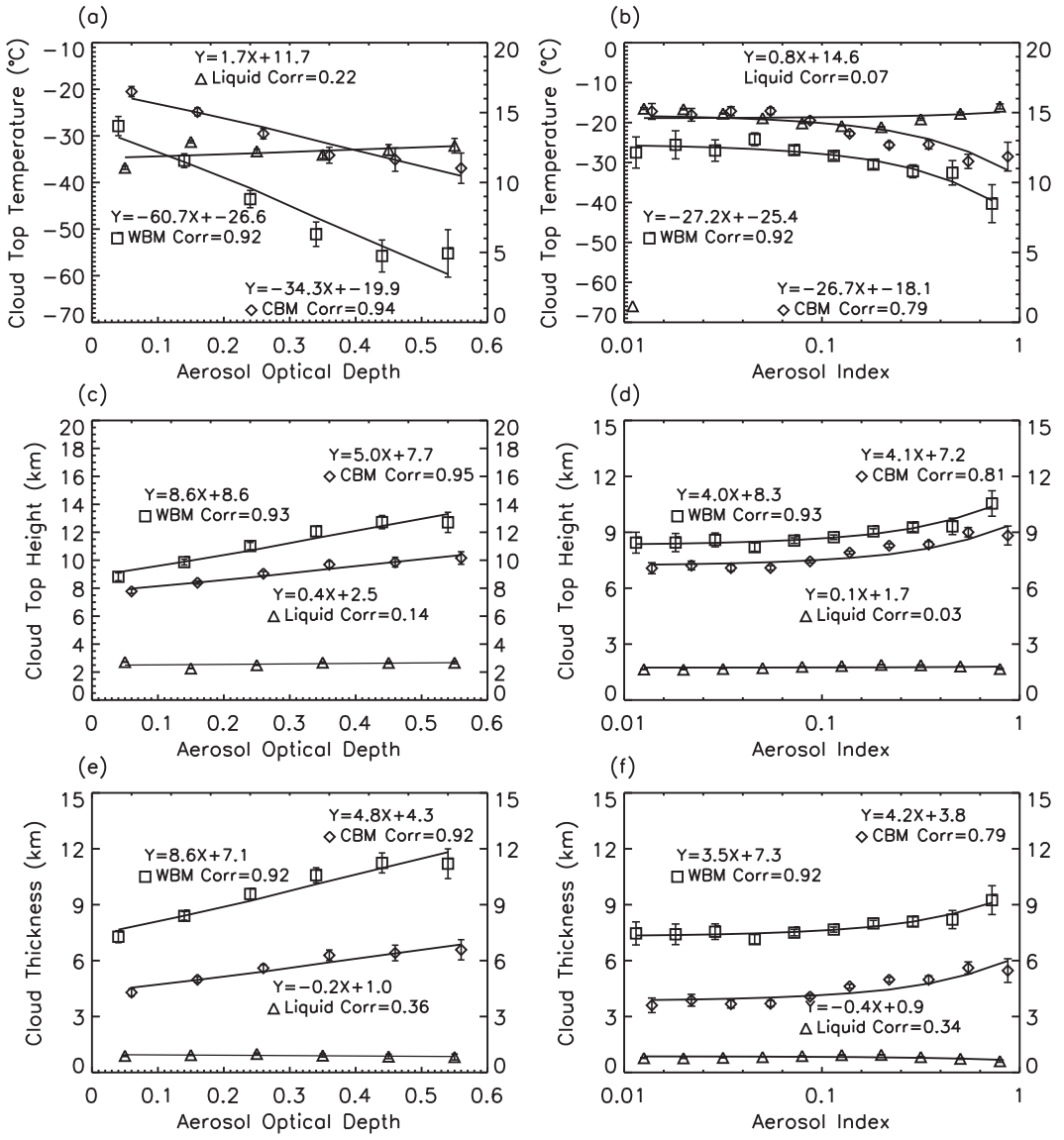

FIG. 1. Cloud macrophysical properties [(top) cloud-top temperature, (middle) cloud-top height, and (bottom) cloud thickness] as functions of (a),(c),(e) AOD over land and (b),(d),(f) AI over oceans. The right-hand *y* axes of all panels are for liquid clouds. Data are shown for liquid clouds (triangles), WBM clouds (squares), and CBM clouds (diamonds). Note that a logarithmic scale is used on the abscissas of (b),(d), and (f).

IWP bins over land and oceans (Fig. 3). The mean IER increases significantly with increasing bin-mean IWP. Within a particular IWP bin, IER is enhanced by aerosols, but the dependence generally becomes weaker with increasing IWP. The finding that an increase in convective strength weakens the positive correlation between IER and AOD (or even reverses the correlation to negative) is shown in both Jiang et al. (2011) and the current study.

Over oceans, the changes are more moderate with a smaller contrast between WBM and CBM clouds (Figs. 2b,d). It follows from Figs. 2a–d that mixed-phase clouds are generally enhanced as aerosol loading increases over both land and oceans. This is, however, not the case for liquid clouds, for which the opposite effect seems to come into play. The mean effective radius of water droplets systematically decreases (from ~11.1 to ~9.8 μm) with increasing aerosol loading. The mean LER for stand-alone liquid clouds and for those beneath mixed-phase clouds are similar over land and oceans, which somewhat attests to the quality of retrievals by the active sensors. The LWPs of WBM clouds decrease with increasing AOD over land and increasing AI over oceans, which is presumably the result of the lifting of

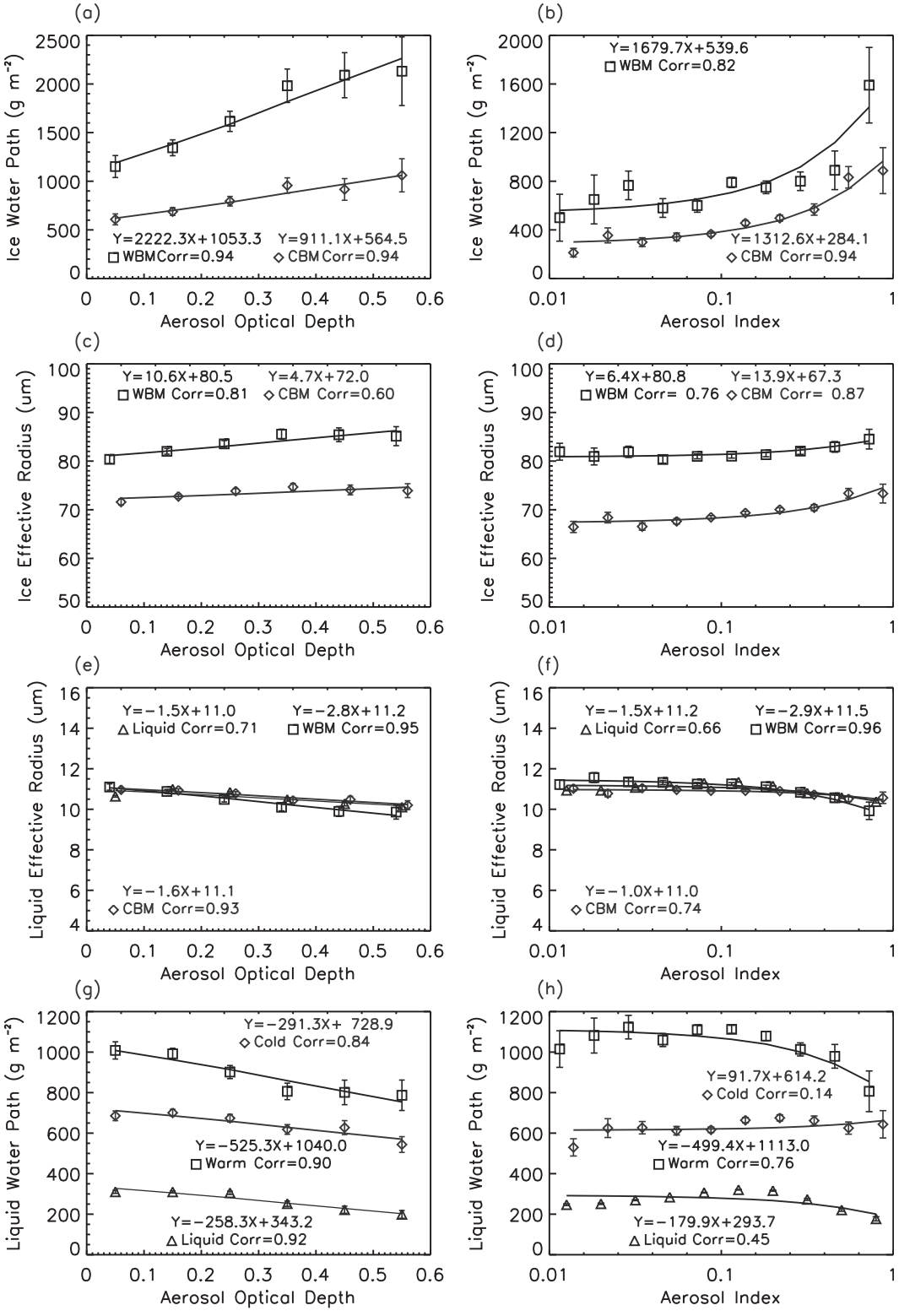

FIG. 2. Cloud microphysical properties [(top)–(bottom) ice water path, ice effective radius, liquid effective radius, and liquid water path] as functions of (a),(c),(e),(g) AOD over land and (b),(d),(f),(h) AI over oceans. Data are shown for liquid clouds (triangles), WBM clouds (squares), and CBM clouds (diamonds). Note that a logarithmic scale is used on the abscissas of (b),(d),(f), and (h).

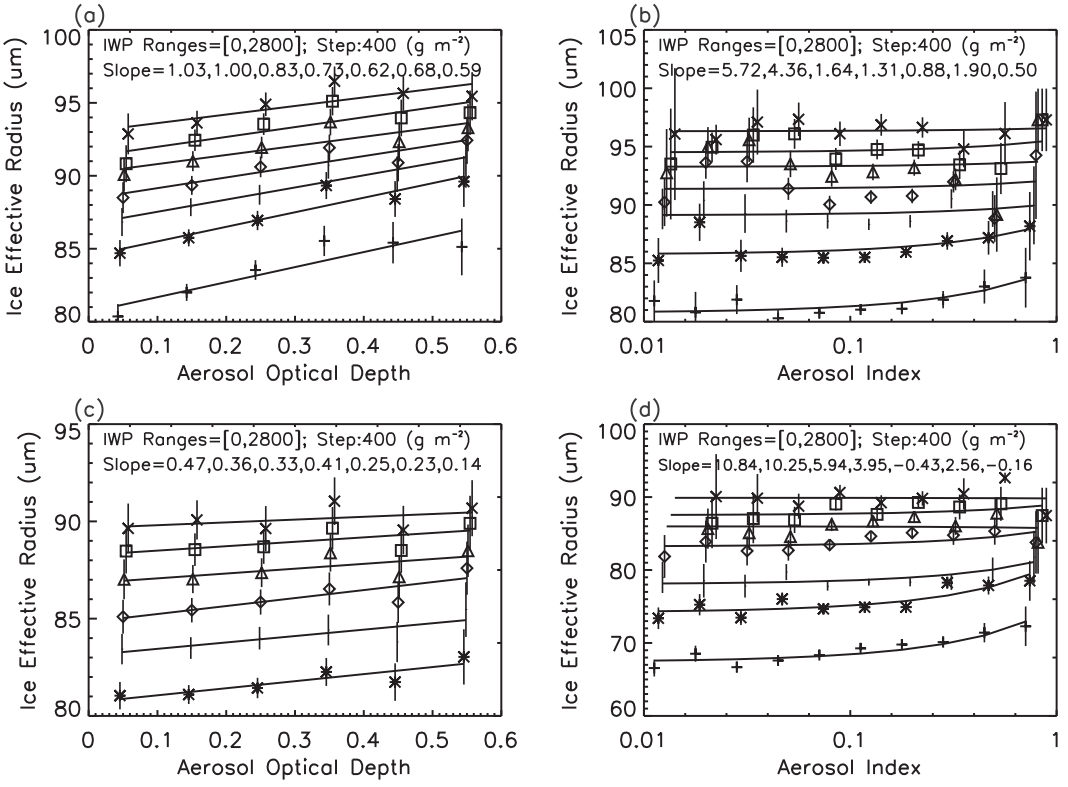

FIG. 3. Ice crystal effective radius in (top) WBM and (bottom) CBM clouds as a function of (a),(c) AOD over land and (b),(d) AI over oceans for different ice water path bins.

liquid droplets through stronger invigoration. While the invigoration of CBM clouds is weaker, the LWP may not always decrease, so a different (but weak) trend is seen over land and oceans. The LWPs of liquid clouds show a weak decreasing trend over land and an even weaker decreasing trend over oceans as aerosol loading increases. The negative correlation between LER and AI and AOD for liquid clouds is a clear manifestation of the first type of AIE because of the competition for moisture, which results in smaller liquid droplets.

Again, such a stark contrast in the response of cloud microphysics (between ice and liquid) to aerosols cannot be explained by large-scale dynamics alone and agrees well with the theories proposed concerning AIEs.

The effect of aerosols on cloud geometry and microphysics undoubtedly affects CRF. SW and LW CRF at the TOA for each *CloudSat* profile are provided based on estimates of fluxes and heating rates using the radiative transfer model described by Stephens et al. (2001). For any grid box with available AOD or AI retrievals, the CRF used is the mean value of the 2B-FLXHR-estimated CRF at the TOA for all single-layer cloudy profiles contained within the grid box.

Figure 4 shows SW CRF (SW-CRF), LW CRF (LW-CRF), and net cloud radiative forcing (NET-CRF) at the TOA as a function of AI over oceans and AOD over land for different cloud types. In general, expected trends in CRF for mixed-phase clouds are seen because the impact of aerosols on cloud geometry and microphysics work in the same direction. This is not so obvious for liquid clouds. For mixed-phase clouds, both SW-CRF and LW-CRF are significantly enhanced by increases in aerosol loading. The trend becomes weaker when AOD becomes larger than 0.3, which is consistent with the trends in cloud microphysical properties (Figs. 2a,c) and macrophysical properties (Figs. 1a,c,e). Since the magnitude of the *y* axis for SW-CRF is much larger than that for LW-CRF, the similar shape of their trends in the figure means that the strength of the SW cooling effect is much larger than that of LW warming. As a result of the dominant role of SW-CRF, the trends in NET-CRF with increases in aerosol loading are similar to those of SW-CRF. SW-CRF ranges from -594 to $-677\,\mathrm{W\,m^{-2}}$ between clean and polluted conditions for WBM clouds, implying a maximum cooling of $83\,\mathrm{W\,m^{-2}}$ due to the AIV. Meanwhile, LW-CRF increases from 85 to $133\,\mathrm{W\,m^{-2}}$, which amounts to an AIV-induced warming of $48\,\mathrm{W\,m^{-2}}$. This offsets the SW cooling and leads to a net cooling of $35\,\mathrm{W\,m^{-2}}$. Table 5 summarizes the SW, LW, and net

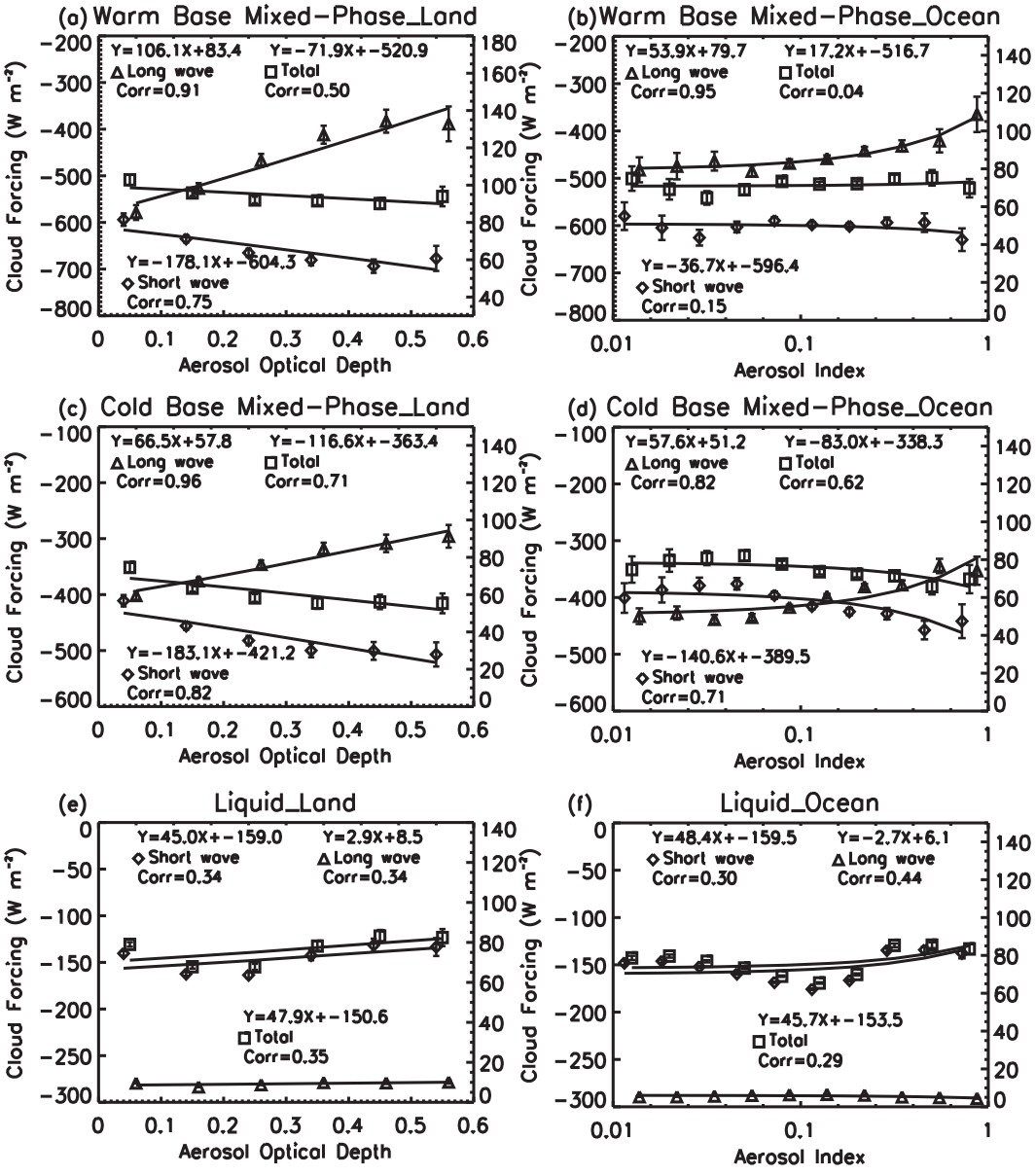

FIG. 4. Cloud radiative forcing (a),(c),(e) over land and (b),(d),(f) over oceans as functions of AOD and AI, respectively, for (a),(b) WBM clouds, (c),(d) CBM clouds, and (e),(f) liquid clouds. The right-hand *y* axes of all panels are for longwave radiative forcing. Data are shown for LW-CRF (triangles), NET-CRF (squares), and SW-CRF (diamonds). Note that a logarithmic scale is used on the abscissas of (b),(d), and (f).

CRF ranges in value for WBM, CBM, and liquid clouds over land and oceans. The magnitudes of CRF differences between clean conditions (lowest AOD and AI bins) and polluted conditions (highest AOD and AI bins) for CBM clouds are generally smaller than those for WBM clouds, and those over oceans are smaller than those over land. Over oceans, the net CRF differences for WBM and CBM clouds are 20 and 17 $W m^{-2}$, respectively, compared with 35 and 64 $W m^{-2}$, respectively, over land.

Results are different for liquid clouds (Figs. 4e,f). The magnitudes of all CRFs are much smaller than their counterparts for mixed-phase clouds, especially for LW-CRF ($<10 W m^{-2}$). This is because of the warm CTT of liquid clouds and their insensitivity to changes in aerosol loading (e.g., Li et al. 2011). SW-CRF varies from -144 to $-133 W m^{-2}$, implying that, despite an apparent nonlinear response, the overall effect of aerosols is warming. When aerosol loading is low (AOD < 0.3 over land or AI < 0.1 over oceans), increases in aerosol

TABLE 5. Shortwave, longwave, and net cloud radiative forcing ($W\,m^{-2}$) of warm-base mixed-phase, cold-base mixed-phase, and liquid clouds for bins with minimum and maximum aerosol loading.

		SW-CRF	LW-CRF	NET-CRF
Warm-base mixed-phase cloud	Land	−594 to −677	85 to 133	−509 to −544
	Ocean	−580 to −630	79 to 109	−501 to −521
Cold-base mixed-phase clouds	Land	−410 to −506	59 to 91	−351 to −415
	Ocean	−400 to −441	50 to 74	−350 to −367
Liquid clouds	Land	−140 to −133	9.6 to 10.1	−130 to −123
	Ocean	−147 to −137	5.3 to 4.5	−142 to −132

loading result in a cooling effect, presumably because of the first type of AIE. This is supported by the increasing LER shown in Figs. 2e and 2f. However, when aerosol loading exceeds the thresholds (i.e., AOD > 0.3 over land or AI > 0.1 over oceans), the warming effect takes over. This switch from cooling to warming is more pronounced over land than over oceans. This is likely because of the two effects at play: the AIE and the aerosol radiative effect, as shown by Koren et al. (2008), using the same threshold of AOD = 0.3. When AOD exceeds this value, the aerosol radiative effect dominates and causes the net warming effect. The type of aerosol present may explain why the nonlinearity, or turnaround, is stronger over land than over oceans. Biomass burning is widespread in the 20°S–20°N band over the Amazon, central Africa, and Southeast Asia. Desert dust is also another dominant aerosol type over land in the tropics. Sea salt particles dominate over the oceans. Absorption by these aerosols is weaker than that by continental aerosols, so the single scattering albedo is stronger (Takemura et al. 2002). Therefore, the switch from cooling to warming that appears over both land and oceans is stronger over land.

AMCRF is calculated as

$$\text{AMCRF(AOD or AI)} = \text{CRF(AOD or AI)} - \text{CRF}_0, \quad (1)$$

where CRF_0 denotes CRF in the absence of aerosols. This can be estimated by extrapolation of the NET-CRF curves shown in Fig. 4. For the land cases, CRF_0 is the y intercept (AOD = 0). It is equal to −521, −363, and $-151\,W\,m^{-2}$ for WBM, CBM, and liquid clouds, respectively. For the ocean cases, CRF_0 is the asymptote of the curves seen in Figs. 4b, 4d, and 4f. It is equal to −517, −338, and $-154\,W\,m^{-2}$ for WBM, CBM, and liquid clouds, respectively. Note that each data point represents the mean CRF, so variability in clouds is taken into account. Changes in cloud properties due to dynamic variability appear to have been effectively smoothed out, resulting in well-behaved functions.

Because the opposite trends imply cooling (low aerosol loading) and warming (high aerosol loading), the sign of the net effect depends on aerosol climatology and the aerosol occurrence frequency. A PDF is needed to determine the climatological-mean AMCRF, which is a function of aerosol loading. Figure 5 shows the PDFs of AOD and AI for WBM and CBM clouds and liquid clouds. The PDFs for the two types of mixed-phase clouds are similar. The peaks for all three cloud types occur in the same AOD bin (0.1–0.2; Fig. 5a). Over oceans, the peak for AI falls in the 0.053–0.081 bin for liquid clouds and in the 0.081–0.123 bin for mixed-phase clouds. Over both oceans and land, there are relatively higher chances of mixed-phase clouds rather than liquid clouds occurring under heavier aerosol loading conditions. It is an open question whether this implies that a polluted environment is more favorable for the development of mixed-phase clouds. In any event, the finding is consistent with the above analyses.

The climatological-mean AMCRF for each cloud type can be determined by summing the CRF weighted by the PDF of AOD or AI as follows:

$$\text{Mean\_AMCRF} = \int_0^1 \text{AMCRF(AOD or AI)PDF}(A)\,dA \quad \text{and} \quad (2)$$

$$\text{Mean\_AMCRF} = \sum_{i=1}^{n} \text{AMCRF}(A_i) f(A_i) \Delta A_i, \quad (3)$$

where A denotes the aerosol loading given either by AOD or AI, and n denotes the number of AOD or AI bins, which is equal to 6 for land and 10 for oceans. The AMCRF for each AOD or AI bin is first weighted by the frequency of aerosol occurrence [Eq. (2)]. The frequency of aerosol occurrence is calculated as the number of samples in each bin divided by the number of samples in all bins. The climatological-mean AMCRF is then calculated as the sum of the weighted AMCRF [Eq. (3)]. Note that the climatological-mean AMCRF is calculated separately for WBM, CBM, and liquid clouds over land and oceans, which are further used to calculate the climatological-mean AMCRF for the entire tropical region over the 4-yr time period (see following two paragraphs).

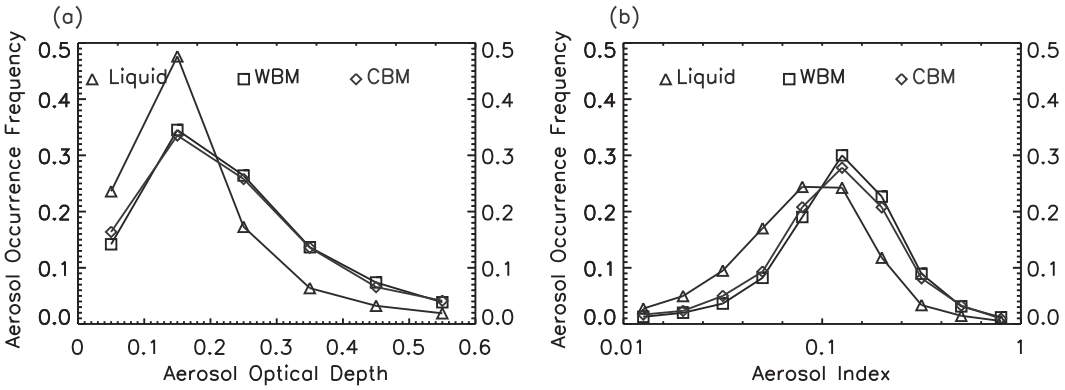

FIG. 5. Aerosol occurrence frequencies for different (a) AOD bins over land and (b) AI bins over oceans. Data are shown for liquid clouds (triangles), WBM clouds (squares), and CBM clouds (diamonds). Note that a logarithmic scale is used on the abscissa of (b).

Figure 6 shows the variation in AMCRF weighted by the PDF of AOD or AI (Weighted-AMCRF) for WBM, CBM, and liquid clouds. The numbers in the figure are the values for SW, LW, and net Weighted-AMCRF (SWW-AMCRF, LWW-AMCRF, and NETW-AMCRF, respectively). Note that those AOD or AI bins with a larger number of samples (i.e., a larger PDF) are more likely to have an impact on Mean_AMCRF and thus will have a larger Weighted-AMCRF. For WBM clouds over land (Fig. 6a), both SWW-AMCRF and LWW-AMCRF increase in magnitude until the 0.2–0.3 AOD bin is reached, then decrease as AOD increases. The Mean_AMCRF (sum of NETW-AMCRF) is $-20.15\,\mathrm{W\,m^{-2}}$. Over oceans (Fig. 6b), the Mean_AMCRF is positive because the sum of LWW-AMCRF is larger than that of SWW-AMCRF. The Weighted-AMCRFs for CBM clouds over land and oceans have distributions similar to those of WBM clouds, but they have relatively stronger SWW-AMCRF, so they lead to more negative Mean_AMCRFs. For liquid clouds over land and oceans, LWW-AMCRF changes little with AOD. The SWW-AMCRF shows decreasing trends over land and oceans, then a switch to increasing trends in the 0.1–0.2 AOD bin over land and in the 0.081–0.123 AI bin over oceans.

The percentage of sample numbers for the three types of clouds (liquid P_l, warm-base mixed-phase P_w, and cold-base mixed-phase P_c) was calculated. The Mean_AMCRF (MAMCRF) over land and oceans is then equal to $\mathrm{MAMCRF_{warm}} \times P_w + \mathrm{MAMCRF_{liquid}} \times P_l + \mathrm{MAMCRF_{cold}} \times P_c$. The net MAMCRF over land and oceans is -2.49 and $-4.72\,\mathrm{W\,m^{-2}}$, respectively. The percentage of sample numbers over land and oceans is 25% and 75%, respectively, so the mean daytime MAMCRF over the entire tropical region is $-4.18\,\mathrm{W\,m^{-2}}$.

Note that the above estimates do not account for the effect of aerosols on the anvils of deep convective clouds, which have a warming effect. As noted in several studies (Koren et al. 2010; Tao et al. 2012; Fan et al. 2013; Yan et al. 2014), aerosols help expand the areal extent of deep convective clouds. This may not only offset the above cooling effect, but may even reverse the total effect from cooling to warming. This effect is not included in this study because of difficulties in identifying anvils using satellite information alone. Because the measured datasets are the outcome of all possible aerosol effects involved (no matter if they are clearly seen in the results or not), the estimated climatological-mean AMCRF reflects the total influence of aerosols, which may not be explained by any individual type of aerosol effect alone. The cooling effect due to SW radiation only occurs during the day, while the LW effect takes place day and night. It is thus possible that the total effect of aerosols on deep convective cloud systems might be warming, as was found by Yan et al. (2014).

The dependence of the above cloud properties on AOD instead of AI for oceans is also investigated. The same trends are seen as when using AI (the dependence of major cloud properties on AOD for oceans is given in Fig. 7) but are slightly weaker over land. Therefore, although AI is the better proxy for CCN than AOD, the results and conclusions of our study are the same no matter which one is used.

Clouds are fundamentally different from region to region within the tropical domain because of meteorological differences. Also, different aerosol types in the tropical region have different physical interactions with clouds. Therefore, regional analyses with varying grid-box sizes (5° × 5°, 10° × 10°, 20° × 20°, and 40° × 40°) are done in order to examine if the significant dependence of the cloud properties of mixed-phase clouds

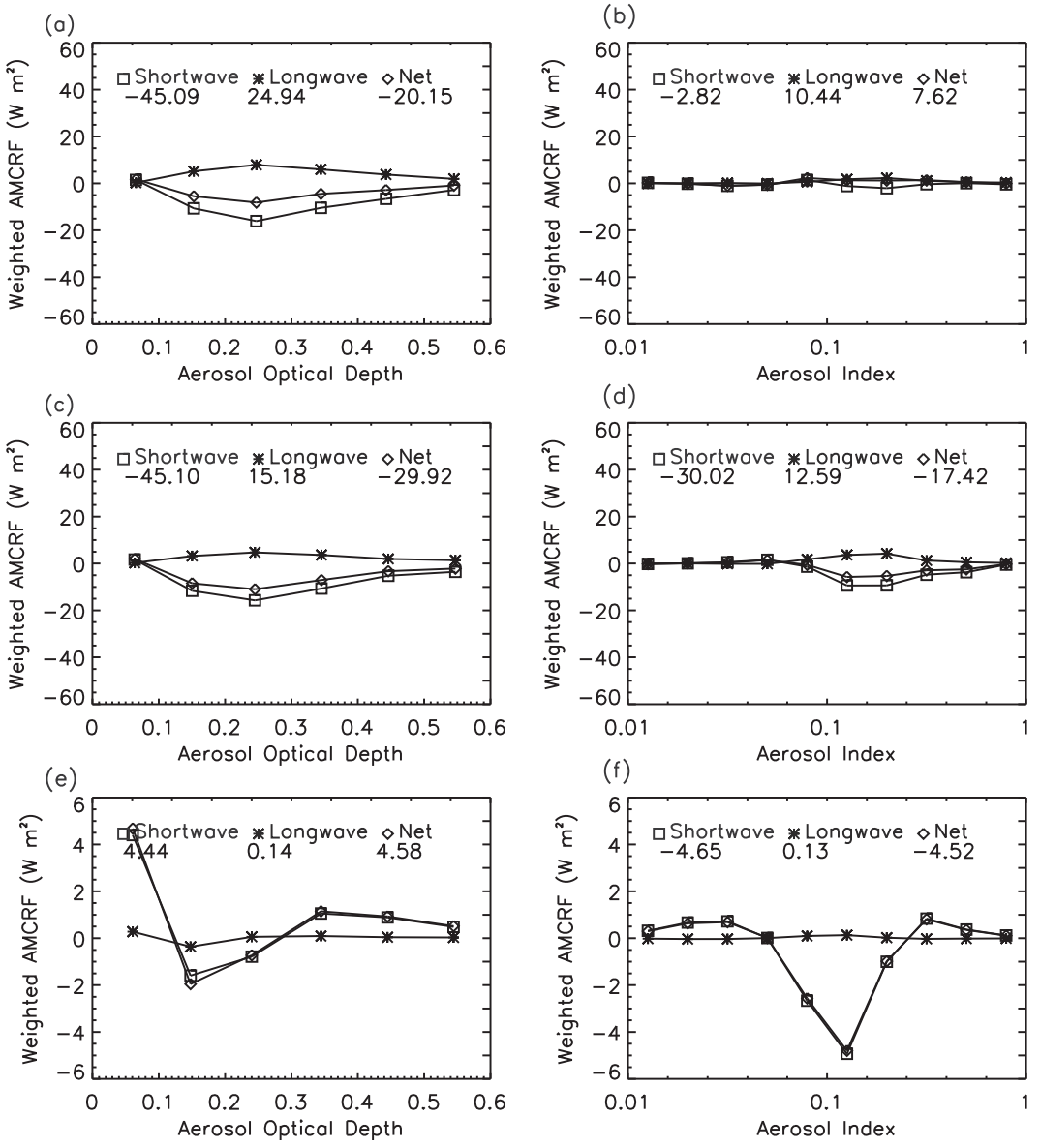

FIG. 6. Aerosol-mediated radiative forcing as functions of (a),(c),(e) AOD over land and (b),(d),(f) AI over oceans for (top) WBM clouds, (middle) CBM clouds, and (bottom) liquid clouds. Mean values of shortwave, longwave, and net radiative forcing ($W\,m^{-2}$) are given in each panel. Note that a logarithmic scale is used on the abscissas of (b),(d), and (f).

(especially WBM clouds) on aerosol loading will change or even be aliased because of differences in aerosol and cloud types.

If the sample number in a grid was 10 or more, the correlations between the CTHs of WBM and AOD and between WBM and AI were calculated. A sample size less than 10 is considered too few to make any meaningful statistical analysis. The spatial distribution of correlation coefficients in each grid was then mapped and is shown in Fig. 8. We find the following: 1) Over land, almost all correlations are positive. Over oceans, there are substantially more areas with positive correlations than negative correlations. This is consistent with the finding that invigoration over oceans is weaker than over land. 2) As the size of the grid boxes increases, the correlation weakens, but positive correlations still dominate. 3) There is no clear geographical dependence found in the distribution of positive and negative correlations. Therefore, although deep clouds over different tropical regions are fundamentally different, the dependence of CTH on aerosol loading seems valid. We believe that the

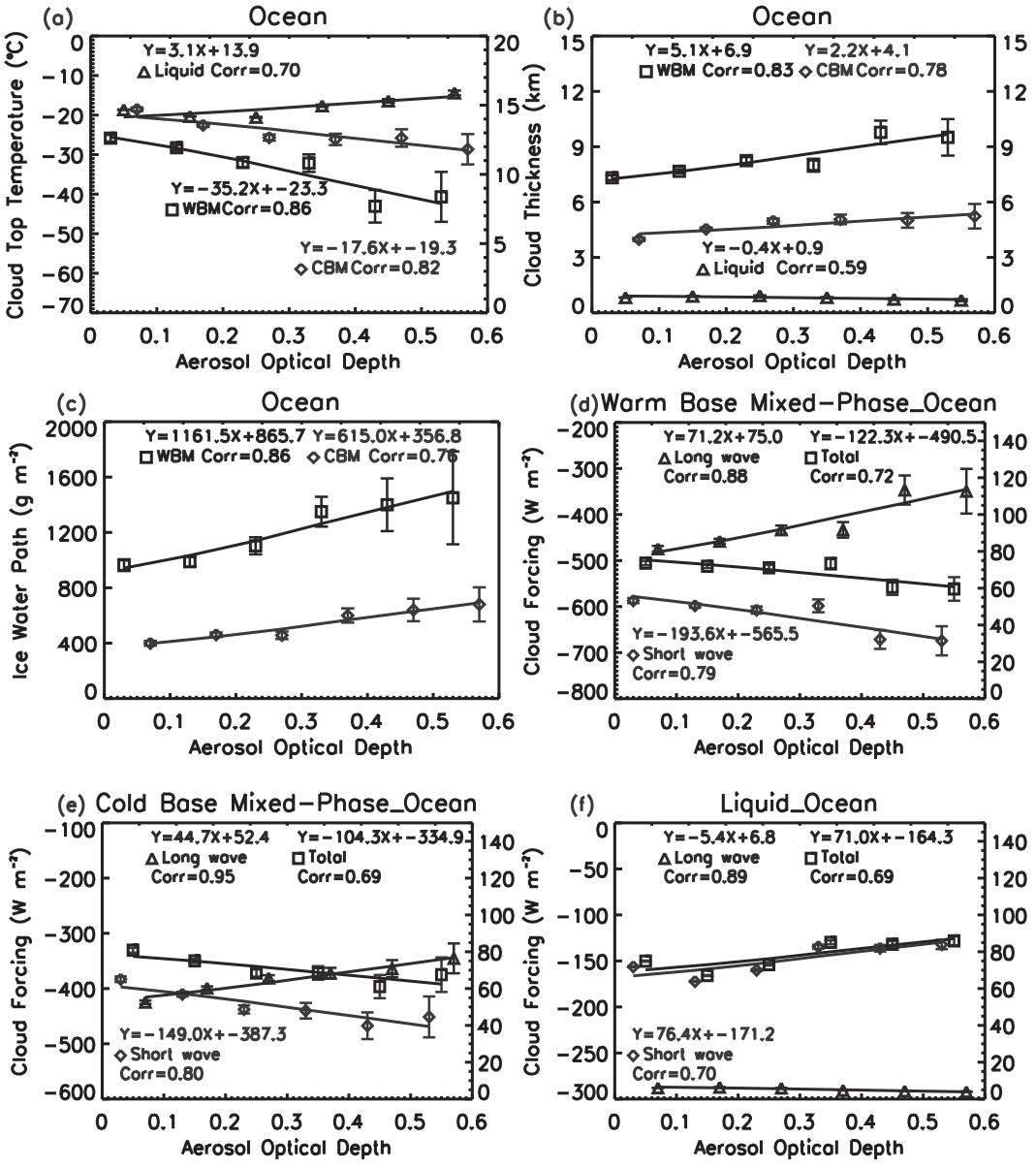

FIG. 7. Major relationships between cloud properties [(a) cloud-top temperature, (b) cloud thickness, (c) ice water path, (d) cloud radiative forcing for WBM clouds, (e) cloud radiative forcing for CBM clouds, and (f) cloud radiative forcing for liquid clouds] and aerosol loading over oceans using AOD.

significant dependence of cloud properties of mixed-phase clouds, especially WBM clouds, on aerosol loading is mainly due to aerosol effects (microphysical and invigoration), although other influences may be at play.

From the perspective of aerosol type, the spatial analysis also gives information about the impact of aerosol type on invigoration. In the northern part of South America and in central Africa, where biomass burning dominates, the positive correlation between CTH and aerosol loading shows a clear evidence of invigoration. A positive correlation is also seen over the Indonesian landmass, where pollution is heavy. Almost no correlation can be seen over the downwind region of North Africa, where dust dominates. Note that AOD data are not available for North Africa and the Arabian Peninsula because the background is too bright for AOD retrievals to be made. For regions where sea salt dominates, correlations can be both positive and negative. The invigoration strength indeed changes with different aerosol types, but overall, tropical aerosols tend to invigorate deep clouds.

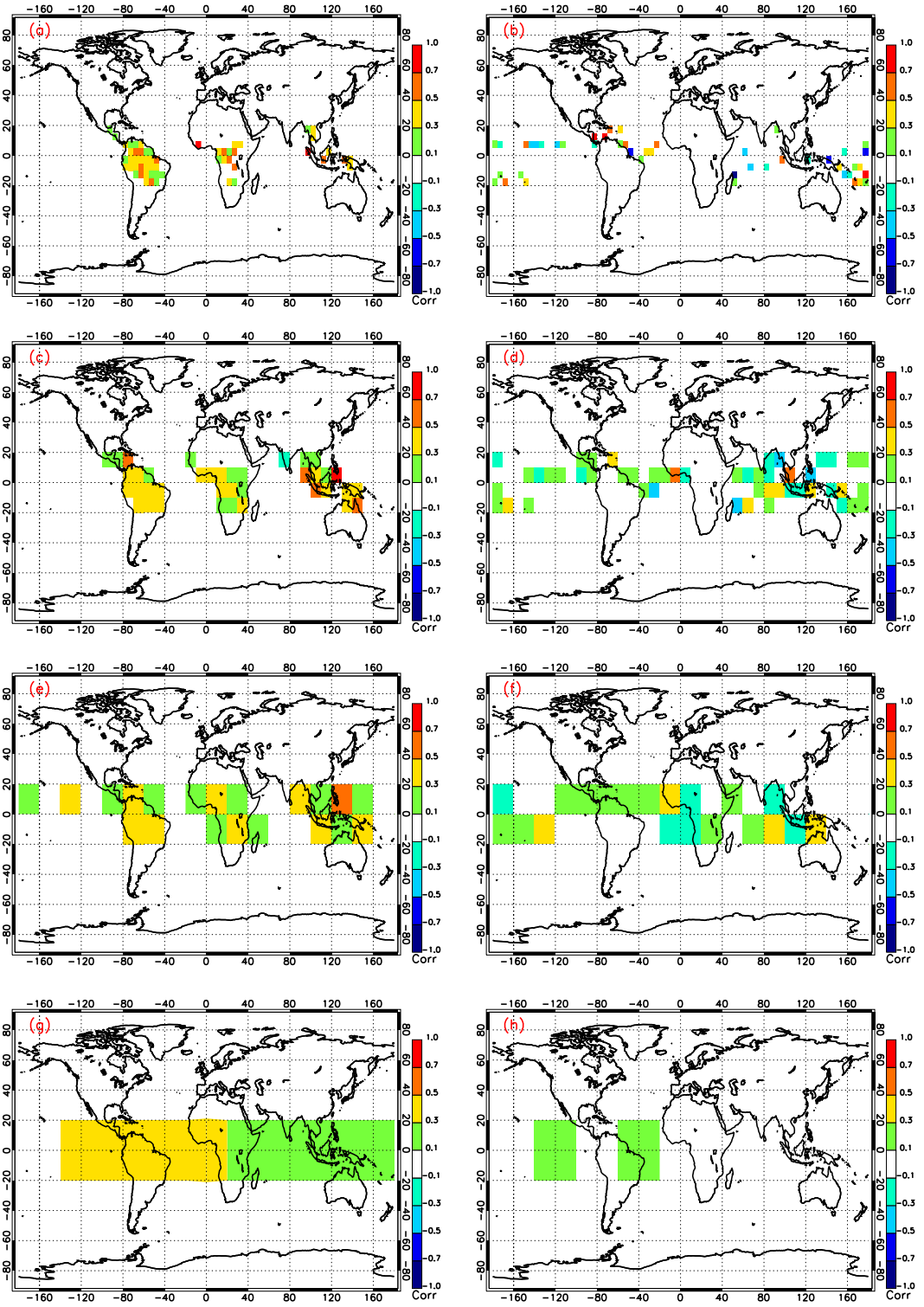

FIG. 8. The geographical distribution of the correlation between cloud-top height of WBM clouds and aerosol loading for different spatial resolutions [(top)–(bottom) 5° × 5°, 10° × 10°, 20° × 20°, and 40° × 40°] over (a),(c),(e),(g) land and (b),(d),(f),(h) oceans. Note that the sample number in each grid is 10 or more.

b. Meteorological influence

The strong coupling between cloud formation and large-scale dynamics is always a challenge in the study of aerosol–cloud interactions. To determine whether the above phenomena are dominated by aerosol–cloud interactions or are driven by a covariance with other meteorological variables, various relationships between meteorological variables relevant to cloud formation and aerosols were examined. Figure 9 shows CWV, relative humidity at 500 hPa (RH500), VaporD, and LTSS as functions of AOD (left column) and AI (right column). The relationships between the water vapor variables and AOD and AI are generally weak, except for the case of liquid clouds over land. The decreasing trend there likely results from statistical uncertainty. If water vapor was the true driver for the correlation between cloud properties and aerosols, positive correlations between the water vapor variables and AOD, which would be stronger over land than over oceans, is expected. This is not the case here. For LTSS, a positive correlation is seen for liquid clouds over land only (Fig. 9e). For mixed-phase clouds, which are sensitive to AOD, all parameters are generally invariant with AI or AOD.

Since there are no simple relationships between the above parameters and cloud properties, we also checked the dependence of CTH, CTK, and IWP on the meteorological parameters. They are correlated with moisture parameters (RH500, CWV, and VaporD). They are also correlated to some degree with LTSS. Figure 10 shows the dependence of CTH on four meteorological parameters. In general, with an increase in moisture, the CTHs of WBM and CBM clouds are significantly enhanced, while the CTHs of liquid clouds increase slightly. Therefore, these meteorological parameters affect the cloud properties investigated in this study. The lack of an obvious correlation between AOD or AI and these meteorological parameters and the significant correlations between AOD or AI and CTH, CTK, IWP, and CRF are likely due to the AIV.

The above analyses are consistent with those conducted using ground-based meteorological variables (Li et al. 2011; Yan et al. 2014) and 1 yr of satellite observations (Niu and Li 2012). Based on the results provided, the significant variations in cloud properties and CRF with AOD and AI shown previously are unlikely to be explained by any of the above meteorological parameters.

4. Conclusions and discussion

Using 4 yr of data from multiple sensors onboard A-Train satellites, a strong impact of the AIV on CRF and related cloud properties for different types of clouds is observed. Both SW-CRF and LW-CRF of mixed-phase clouds are enhanced. For liquid clouds, the correlations between SW-CRF and AI and between SW-CRF and AOD are positive, then negative. Variations in cloud macrophysical and microphysical properties with AI and AOD suggest that the above findings result from a combination of the AIV, the ''Twomey effect,'' and the ''semidirect effect.''

For mixed-phase clouds, cloud-top height, cloud depth, and ice processing in clouds are significantly enhanced with increasing AI and AOD via the AIV. More SW radiation is reflected back to space, resulting in a stronger SW-CRF, and more LW radiation from the surface is captured and redistributed within the atmosphere, resulting in a stronger LW-CRF. For liquid clouds, cloud geometry shows no obvious change with AI and AOD, resulting in a constant LW-CRF. The variation in SW-CRF seems dominated by a combination of the Twomey effect and the semidirect effect. The dependencies of meteorological variables on AI and AOD found in this study and reported in other studies do not suggest any dominant role played by a third factor.

Potential uncertainties, such as retrieval uncertainties and the inherent limitations of polar-orbiting satellite measurements, make it difficult to demonstrate causal relationships between CRF and AI or AOD. Fortunately, many physical mechanisms in support of the findings in this study have been demonstrated in several modeling studies, such as Fan et al. (2013). However, modeling studies cannot generate the climatological values estimated in this study. If they truly reflect the influence of aerosols, the estimates made here may be valuable for the validation of modeling results concerning the impact of aerosols on Earth's radiation budget.

Acknowledgments. This work is financially supported by the Key State Basic Research Development Program of China on Global Change (2013CB955804; 2011CB403405); the Public Meteorology Special Foundation of MOST (GYHY210406023); the National Natural Science Foundation of China (41375080); the National Science Foundation of the United States (AGS1118325) and China (41175019); and the ESPRE (2015-TDZD-090). The authors thank the NASA Goddard Earth Sciences Distributed Active Archive Centers for providing the MODIS data, the NASA *CloudSat* project for providing the *CloudSat* data, and the NASA Langley Atmospheric Science Data Center for providing the *CALIPSO* data used in this study.

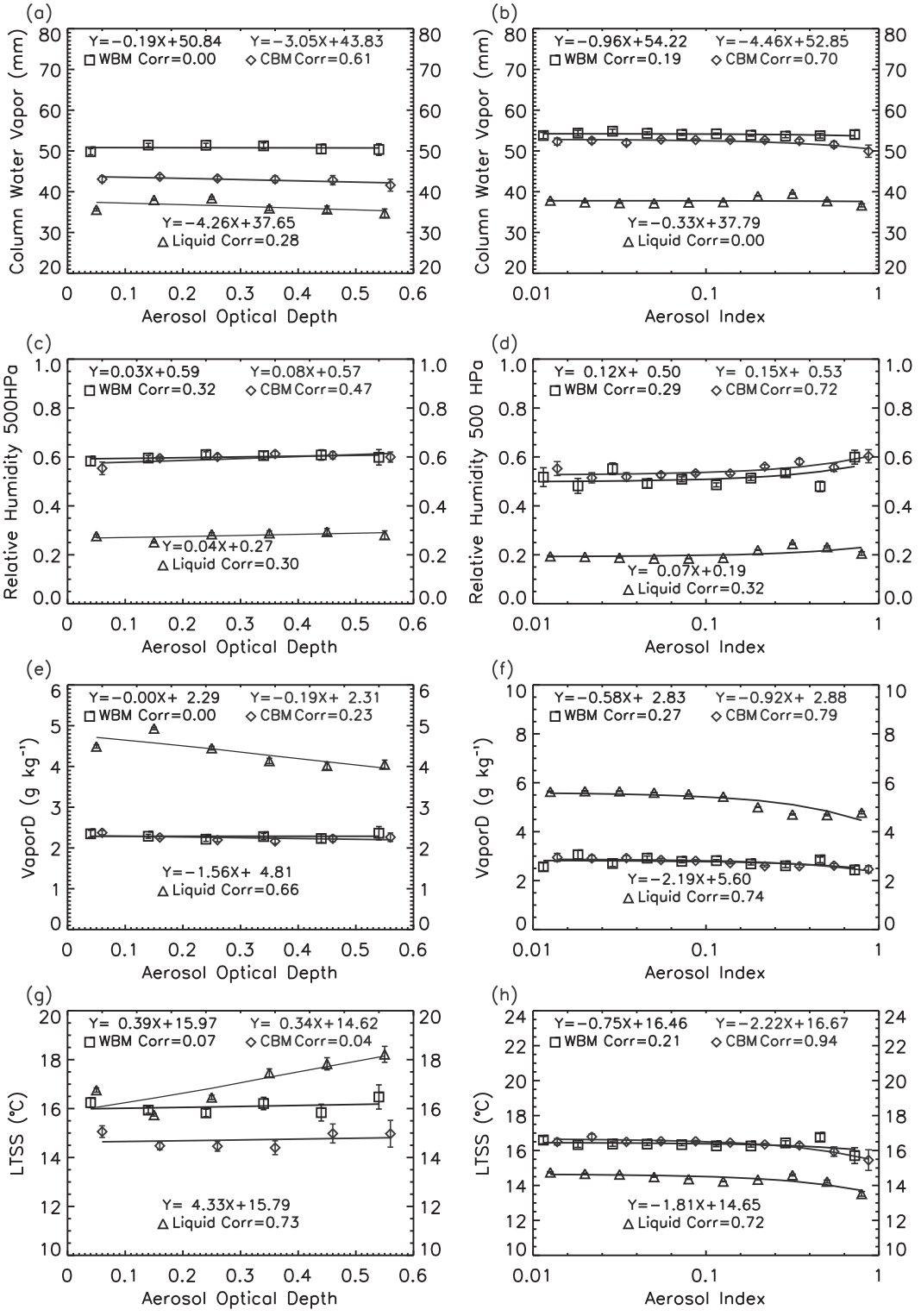

FIG. 9. Meteorological parameters [(top)–(bottom) column water vapor, relative humidity at 500 hPa, VaporD, and LTSS] as functions of (a),(c),(e),(g) AOD over land and (b),(d),(f),(h) AI over oceans. Data are shown for liquid clouds (triangles), WBM clouds (squares), and CBM clouds (diamonds). Note that a logarithmic scale is used on the abscissas of (b),(d),(f), and (h).

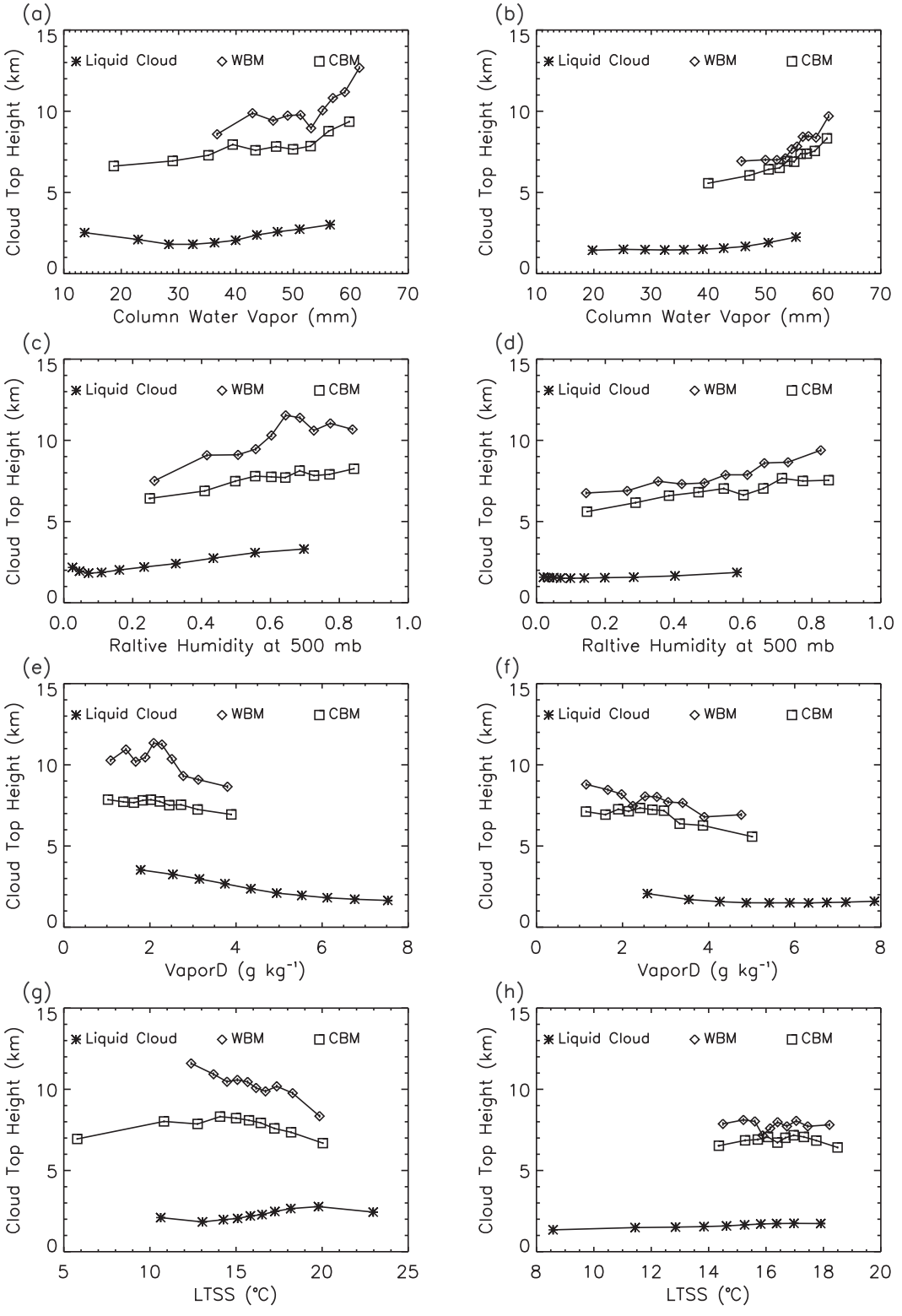

FIG. 10. Cloud-top height as functions of meteorological parameters [(top)–(bottom) column water vapor, relative humidity at 500 hPa, VaporD, and LTSS] over (a),(c),(e),(g) land and (b),(d),(f),(h) oceans. Data are shown for liquid clouds (asterisks), CBM clouds (squares), and WBM clouds (diamonds). The error bar is the standard error. Each bin contains 10% of the total number of samples sorted by meteorological parameter. The number of samples in each bin for liquid, CBM, and WBM clouds is 3461, 687, and 323, respectively, over land and 12 570, 387, and 200, respectively, over oceans.

REFERENCES

Albrecht, B., 1989: Aerosols, cloud microphysics, and fractional cloudiness. *Science*, **245**, 1227–1230, doi:10.1126/science.245.4923.1227.

Andreae, M. O., D. Rosenfeld, P. Artaxo, A. A. Costa, G. P. Frank, K. M. Longo, and M. A. F. Silva-Dias, 2004: Smoking rain clouds over the Amazon. *Science*, **303**, 1337–1342, doi:10.1126/science.1092779.

Bell, T. L., D. Rosenfeld, and K. M. Kim, 2009: Weekly cycle of lightning: Evidence of storm invigoration by pollution. *Geophys. Res. Lett.*, **36**, L23805, doi:10.1029/2009GL040915.

Camponogara, G., M. A. F. Silva Dias, and G. G. Carrio, 2014: Relationship between Amazon biomass burning aerosols and rainfall over the La Plata Basin. *Atmos. Chem. Phys.*, **14**, 4397–4407, doi:10.5194/acp-14-4397-2014.

Chu, D. A., and Coauthors, 2005: Evaluation of aerosol properties over ocean from Moderate Resolution Imaging Spectroradiometer (MODIS) during ACE-Asia. *J. Geophys. Res.*, **110**, D07308, doi:10.1029/2004JD005208.

Fan, J. W., R. Y. Zhang, G. H. Li, and W. K. Tao, 2007: Effects of aerosols and relative humidity on cumulus clouds. *J. Geophys. Res.*, **112**, D14204, doi:10.1029/2006JD008136.

——, and Coauthors, 2009: Dominant role by vertical wind shear in regulating aerosol effects on deep convective clouds. *J. Geophys. Res.*, **114**, D22206, doi:10.1029/2009JD012352.

——, D. Rosenfeld, Y. N. Ding, L. R. Leung, and Z. Q. Li, 2012: Potential aerosol indirect effects on atmospheric circulation and radiative forcing through deep convection. *Geophys. Res. Lett.*, **39**, L09806, doi:10.1029/2012GL051851.

——, L. R. Leung, D. Rosenfeld, Q. Chen, Z. Q. Li, J. Q. Zhang, and H. R. Yan, 2013: Microphysical effects determine macrophysical response for aerosol impacts on deep convective clouds. *Proc. Natl. Acad. Sci. USA*, **110**, E4581–E4590, doi:10.1073/pnas.1316830110.

Feingold, G., R. Furrer, P. Pilewskie, L. A. Remer, Q. L. Min, and H. Jonsson, 2006: Aerosol indirect effect studies at Southern Great Plains during the May 2003 Intensive Operations Period. *J. Geophys. Res.*, **111**, D05S14, doi:10.1029/2004JD005648.

Freud, E., and D. Rosenfeld, 2012: Linear relation between convective cloud drop number concentration and depth for rain initiation. *J. Geophys. Res.*, **117**, D02207, doi:10.1029/2011JD016457.

Jiang, J. H., and Coauthors, 2011: Influence of convection and aerosol pollution on ice cloud particle effective radius. *Atmos. Chem. Phys.*, **11**, 457–463, doi:10.5194/acp-11-457-2011.

Khain, A. P., and A. Pokrovsky, 2004: Simulation of effects of atmospheric aerosols on deep turbulent convective clouds using a spectral microphysics mixed-phase cumulus cloud model. Part II: Sensitivity study. *J. Atmos. Sci.*, **61**, 2983–3001, doi:10.1175/JAS-3281.1.

——, D. Rosenfeld, and A. Pokrovsky, 2005: Aerosol impact on the dynamics and microphysics of deep convective clouds. *Quart. J. Roy. Meteor. Soc.*, **131**, 2639–2663, doi:10.1256/qj.04.62.

——, N. BenMoshe, and A. Pokrovsky, 2008: Factors determining the impact of aerosols on surface precipitation from clouds: An attempt at classification. *J. Atmos. Sci.*, **65**, 1721–1748, doi:10.1175/2007JAS2515.1.

Klein, S. A., and D. L. Hartmann, 1993: The seasonal cycle of low stratiform clouds. *J. Climate*, **6**, 1587–1606, doi:10.1175/1520-0442(1993)006<1587:TSCOLS>2.0.CO;2.

Koren, I., Y. J. Kaufman, D. Rosenfeld, L. A. Remer, and Y. Rudich, 2005: Aerosol invigoration and restructuring of Atlantic convective clouds. *Geophys. Res. Lett.*, **32**, L14828, doi:10.1029/2005GL023187.

——, J. V. Martins, L. A. Remer, and H. Afargan, 2008: Smoke invigoration versus inhibition of clouds over the Amazon. *Science*, **321**, 946–949, doi:10.1126/science.1159185.

——, L. A. Remer, O. Altaratz, J. V. Martins, and A. David, 2010: Aerosol-induced changes of convective cloud anvils produce strong climate warming. *Atmos. Chem. Phys.*, **10**, 5001–5010, doi:10.5194/acp-10-5001-2010.

L'Ecuyer, T. S., and J. H. Jiang, 2010: Touring the atmosphere aboard the A-Train. *Phys. Today*, **63**, 36–41, doi:10.1063/1.3463626.

Levy, R. C., L. A. Remer, S. Mattoo, E. F. Vermote, and Y. J. Kaufman, 2007: Second-generation operational algorithm: Retrieval of aerosol properties over land from inversion of Moderate Resolution Imaging Spectroradiometer spectral reflectance. *J. Geophys. Res.*, **112**, D13211, doi:10.1029/2006JD007811.

——, ——, R. G. Kleidman, S. Mattoo, C. Ichoku, R. Kahn, and T. F. Eck, 2010: Global evaluation of the Collection 5 MODIS dark-target aerosol products over land. *Atmos. Chem. Phys.*, **10**, 10 399–10 420, doi:10.5194/acp-10-10399-2010.

Li, Z. Q., F. Niu, K.-H. Lee, J. Y. Xin, W. M. Hao, B. Nordgren, Y. S. Wang, and P. C. Wang, 2007: Validation and understanding of Moderate Resolution Imaging Spectroradiometer aerosol products (C5) using ground-based measurements from the handheld Sun photometer network in China. *J. Geophys. Res.*, **112**, D22S07, doi:10.1029/2007JD008479.

——, ——, J. W. Fan, Y. G. Liu, D. Rosenfeld, and Y. N. Ding, 2011: Long-term impacts of aerosols on the vertical development of clouds and precipitation. *Nat. Geosci.*, **4**, 888–894, doi:10.1038/ngeo1313.

Lin, J. C., T. Matsui, R. A. Pielke Sr., and C. Kummerow, 2006: Effects of biomass-burning-derived aerosols on precipitation and clouds in the Amazon Basin: A satellite-based empirical study. *J. Geophys. Res.*, **111**, D19204, doi:10.1029/2005JD006884.

Lohmann, U., and J. Feichter, 2005: Global indirect aerosol effects: A review. *Atmos. Chem. Phys.*, **5**, 715–737, doi:10.5194/acp-5-715-2005.

Marshak, A., G. Y. Wen, J. A. Coakley Jr., L. A. Remer, N. G. Loeb, and R. F. Cahalan, 2008: A simple model for the cloud adjacency effect and the apparent bluing of aerosols near clouds. *J. Geophys. Res.*, **113**, D14S17, doi:10.1029/2007JD009196.

Mi, W., Z. Q. Li, X. G. Xia, B. Holben, R. Levy, F. S. Zhao, H. B. Chen, and M. Cribb, 2007: Evaluation of the Moderate Resolution Imaging Spectroradiometer aerosol products at two Aerosol Robotic Network stations in China. *J. Geophys. Res.*, **112**, D22S08, doi:10.1029/2007JD008474.

Nakajima, T., A. Higurashi, K. Kawamoto, and J. E. Penner, 2001: A possible correlation between satellite-derived cloud and aerosol microphysical parameters. *Geophys. Res. Lett.*, **28**, 1171–1174, doi:10.1029/2000GL012186.

NASA CloudSat Project, 2007: 2B-GEOPROF-LIDAR, 2B-CWC-RVOD, 2B-FLXHR, and ECMWF-AUX, R04. CloudSat Data Processing Center, accessed 1 March 2012. [Available online at http://www.cloudsat.cira.colostate.edu/.]

NASA Goddard Space Flight Center, 2008: MYD08, Collection 5.1. Level 1 and Atmosphere Archive and Distribution System, accessed 1 April 2012. [Available online at https://ladsweb.nascom.nasa.gov/data/search.html.]

Niu, F., and Z. Q. Li, 2012: Systematic variations of cloud top temperature and precipitation rate with aerosols over the global tropics. *Atmos. Chem. Phys.*, **12**, 8491–8498, doi:10.5194/acp-12-8491-2012.

Peng, J., H. Zhang, and Z. Q. Li, 2014: Temporal and spatial variations of global deep cloud systems based on CloudSat and CALIPSO satellite observations. *Adv. Atmos. Sci.*, **31**, 593–603, doi:10.1007/s00376-013-3055-6.

Ramaswamy, V., and Coauthors, 2001: Radiative forcing of climate change. *Climate Change 2001: The Scientific Basis*, J. T. Houghton et al., Eds., Cambridge University Press, 349–416. [Available online at http://www.grida.no/climate/ipcc_tar/wg1/pdf/TAR-06.pdf.]

Redelsperger, J. L., D. B. Parsons, and F. Guichard, 2002: Recovery processes and factors limiting cloud-top height following the arrival of a dry intrusion observed during TOGA COARE. *J. Atmos. Sci.*, **59**, 2438–2457, doi:10.1175/1520-0469(2002)059<2438:RPAFLC>2.0.CO;2.

Rosenfeld, D., and T. L. Bell, 2011: Why do tornados and hailstorms rest on weekends? *J. Geophys. Res.*, **116**, D20211, doi:10.1029/2011JD016214.

——, Y. J. Kaufman, and I. Koren, 2006: Switching cloud cover and dynamical regimes from open to closed Benard cells in response to the suppression of precipitation by aerosols. *Atmos. Chem. Phys.*, **6**, 2503–2511, doi:10.5194/acp-6-2503-2006.

——, A. Khain, B. Lynn, and W. L. Woodley, 2007: Simulation of hurricane response to suppression of warm rain by sub-micron aerosols. *Atmos. Chem. Phys.*, **7**, 3411–3424, doi:10.5194/acp-7-3411-2007.

——, U. Lohmann, G. B. Raga, C. D. O'Dowd, M. Kulmala, S. Fuzzi, A. Reissell, and M. O. Andreae, 2008a: Flood or drought: How do aerosols affect precipitation? *Science*, **321**, 1309–1313, doi:10.1126/science.1160606.

——, W. L. Woodley, D. Axisa, E. Freud, J. G. Hudson, and A. Givati, 2008b: Aircraft measurements of the impacts of pollution aerosols on clouds and precipitation over the Sierra Nevada. *J. Geophys. Res.*, **113**, D15203, doi:10.1029/2007JD009544.

——, M. Clavner, and R. Nirel, 2011: Pollution and dust aerosols modulating tropical cyclones intensities. *Atmos. Res.*, **102**, 66–76, doi:10.1016/j.atmosres.2011.06.006.

——, W. L. Woodley, A. Khain, W. R. Cotton, G. Carrio, I. Ginis, and J. H. Golden, 2012: Aerosol effects on microstructure and intensity of tropical cyclones. *Bull. Amer. Meteor. Soc.*

——, R. Wood, L. J. Donner, and S. Sherwood, 2013: Aerosol cloud-mediated radiative forcing: Highly uncertain and opposite effects from shallow and deep clouds. *Climate Science for Serving Society: Research, Modeling and Prediction Priorities*, G. R. Asrar and J. W. Hurrell, Eds., Springer, 105–149, doi:10.1007/978-94-007-6692-1_5.

Seifert, A., and K. D. Beheng, 2006: A two-moment cloud microphysics parameterization for mixed-phase clouds. Part 2: Maritime vs. continental deep convective storms. *Meteor. Atmos. Phys.*, **92**, 67–82, doi:10.1007/s00703-005-0113-3.

Stephens, G. L., P. M. Gabriel, and P. T. Partain, 2001: Parameterization of atmospheric radiative transfer. Part I: Validity of simple models. *J. Atmos. Sci.*, **58**, 3391–3409, doi:10.1175/1520-0469(2001)058<3391:POARTP>2.0.CO;2.

Storer, R. L., S. C. Van den Heever, and T. S. L'Ecuyer, 2014: Observations of aerosol-induced convective invigoration in the tropical east Atlantic. *J. Geophys. Res. Atmos.*, **119**, 3963–3975, doi:10.1002/2013JD020272.

Takemura, T., T. Nakajima, O. Dubovik, B. N. Holben, and S. Kinne, 2002: Single-scattering albedo and radiative forcing of various aerosol species with a global three-dimensional model. *J. Climate*, **15**, 333–352, doi:10.1175/1520-0442(2002)015<0333:SSAARF>2.0.CO;2.

Tao, W. K., X. W. Li, A. Khain, T. Matsui, S. Lang, and J. Simpson, 2007: Role of atmospheric aerosol concentration on deep convective precipitation: Cloud-resolving model simulations. *J. Geophys. Res.*, **112**, D24S18, doi:10.1029/2007JD008728.

——, J. P. Chen, Z. Q. Li, C. E. Wang, and C. D. Zhang, 2012: Impact of aerosols on convective clouds and precipitation. *Rev. Geophys.*, **50**, RG2001, doi:10.1029/2011RG000369.

Ten Hoeve, J. E., M. Z. Jacobson, and L. A. Remer, 2012: Comparing results from a physical model with satellite and in situ observations to determine whether biomass burning aerosols over the Amazon brighten or burn off clouds. *J. Geophys. Res.*, **117**, D08203, doi:10.1029/2011JD016856.

Twomey, S., 1977: The influence of pollution on the shortwave albedo of clouds. *J. Atmos. Sci.*, **34**, 1149–1152, doi:10.1175/1520-0469(1977)034<1149:TIOPOT>2.0.CO;2.

Van den Heever, S. C., G. L. Stephens, and N. B. Wood, 2011: Aerosol indirect effects on tropical convection characteristics under conditions of radiative–convective equilibrium. *J. Atmos. Sci.*, **68**, 699–718, doi:10.1175/2010JAS3603.1.

Varnai, T., and M. Alexander, 2011: Global CALIPSO observations of aerosol changes near clouds. *IEEE Trans. Geosci. Remote Sens.*, **8**, 19–23, doi:10.1109/LGRS.2010.2049982.

Wang, C., 2005: A modeling study of the response of tropical deep convection to the increase of cloud condensation nuclei concentration: 1. Dynamics and microphysics. *J. Geophys. Res.*, **110**, D21211, doi:10.1029/2004JD005720.

Wang, Y., R. Y. Zhang, and R. Saravanan, 2014: Asian pollution climatically modulates mid-latitude cyclones following hierarchical modelling and observational analysis. *Nat. Commun.*, **5**, 3098, doi:10.1038/ncomms4098.

Wen, G. Y., A. Marshak, R. F. Cahalan, L. A. Remer, and R. G. Kleidman, 2007: 3-D aerosol-cloud radiative interaction observed in collocated MODIS and ASTER images of cumulus cloud fields. *J. Geophys. Res.*, **112**, D13204, doi:10.1029/2006JD008267.

Yan, H. R., Z. Q. Li, J. P. Huang, M. Cribb, and J. J. Liu, 2014: Long-term aerosol-mediated changes in cloud radiative forcing of deep clouds at the top and bottom of the atmosphere over the Southern Great Plains. *Atmos. Chem. Phys.*, **14**, 7113–7124, doi:10.5194/acp-14-7113-2014.

Yang, W. D., A. Marshak, T. Várnai, and Z. Y. Liu, 2012: Effect of CALIPSO cloud–aerosol discrimination (CAD) confidence levels on observations of aerosol properties near clouds. *Atmos. Res.*, **116**, 134–141, doi:10.1016/j.atmosres.2012.03.013.

Yang, X., and Z. Q. Li, 2014: Increases in thunderstorm activity and relationships with air pollution in southeast China. *J. Geophys. Res. Atmos.*, **119**, 1835–1844, doi:10.1002/2013JD021224.

——, M. Ferrat, and Z. Q. Li, 2013a: New evidence of orographic precipitation suppression by aerosols in central China. *Meteor. Atmos. Phys.*, **119**, 17–29, doi:10.1007/s00703-012-0221-9.

——, Z. Y. Yao, Z. Q. Li, and T. Y. Fan, 2013b: Heavy air pollution suppresses summer thunderstorms in central China. *J. Atmos. Sol.-Terr. Phys.*, **95–96**, 28–40, doi:10.1016/j.jastp.2012.12.023.